ELSEVIER

Thermochimica Acta 282/283 (1996) 305–316

thermochimica acta

The oxidation of violarite[1]

J.G. Dunn*, V.L. Howes

School of Applied Chemistry, Curtin University, Perth, Western Australia, Australia

Abstract

A sample of violarite was synthesized from pure components and characterized. Samples of particle size 45–75 μm were oxidized in a TG–DTA apparatus at a heating rate of 10°C min^{-1} and the products characterized at various temperatures by X-ray diffraction (XRD), backscattered electron (BSE) images obtained on a Scanning Electron Microscope (SEM), Fourier transform infrared (FT–IR) spectroscopy and electronprobe microanalysis (EPMA).

Only minor sulfation reactions occurred up to 405°C, but above this temperature the violarite decomposed to form a monosulfide solid solution (mss, $(Fe,Ni)_{1-x}S$) and sulfur. The first reaction produced a mass loss, and oxidation of the evolved sulfur produced an exotherm. From 470°C, there was a mass gain due to the continued formation of sulfate species and an exotherm caused by the conversion of iron sulfide to hematite. From 585°C, a mass loss occurred as the iron sulfates decomposed. At 670°C decomposition of the mss took place, with the formation of heazlewoodite, $(Ni,Fe)_{3\pm x}S_2$, and sulfur. The first reaction produced a mass loss, and oxidation of the evolved sulfur gave an exotherm. Trevorite, $(Fe,Ni)_3O_4$, was also formed above this temperature, from the oxidation of either mss or heazlewoodite, and this reaction also contributed to the mass loss. Above 725°C a mass loss and sulfur dioxide evolution was associated with the decomposition of nickel sulfate. This was followed by an endotherm at 785°C caused by the melting of the heazlewoodite, which immediately oxidized to produce a mass loss and exotherm. The final product above 860°C contained trevorite, nickel oxide and hematite. Extensive migration of iron occurred during the oxidation process.

Keywords: Violarite; Oxidation; XRD; BSE; SEM; FT–IR; EPMA

1. Introduction

Violarite, with an ideal formula of $FeNi_2S_4$, is a nickel–iron sulfide of economic importance since it is a component in the nickel sulfide concentrate used as feed stock in

* Corresponding author.

[1] Dedicated to Takeo Ozawa on the Occasion of his 65th Birthday.

SSDI 0040-6031(96)02806-7

a flash smelting process to produce nickel matte. The mineral is very common in several developed nickel sulfide deposits in Western Australia and in some cases is the predominant nickel mineral [1].

Previous studies on violarite have focussed on phase stabilities in evacuated, heated, sealed tubes in which the solid is in equilibrium with sulfur vapor [2, 3]. The maximum thermal stability for violarite was found to be 461°C, with a composition of $Fe_{0.92}Ni_{2.08}S_4$ [3]. As the system becomes more nickel-rich, the decomposition temperature decreases, eventually reaching 356°C at Ni_3S_4. Beyond these temperatures, violarite decomposes to form monosulfide solid solution (mss), of general formula $(Fe, Ni)_{1-x}S$, pyrite (FeS_2), and vaesite (NiS_2). The last two compounds can be substituted by Ni and Fe, respectively. Further loss of sulfur occurs above 650°C with the formation of heazlewoodite (Ni_3S_2).

In natural geological systems, violarite is formed by the supergene alteration of mixtures of iron–nickel sulfides and hence occurs in complex assemblages intimately mixed with other sulfides, oxidation products and gangue minerals [4, 5]. Because these other products have properties in common with violarite, we have not found it possible to separate a pure sample of violarite from its host matrix [6]. Consequently we have synthesized a sample of violarite from pure elements in order to study its oxidative behavior without the influence of these other minerals.

2. Experimental

2.1. Preparation of synthetic violarite, $FeNi_2S_4$

Violarite of ideal stoichiometry was prepared in a two-step process as described by Craig [3]. A monosulfide solid solution (mss) was prepared with the formula $Fe_{0.28}Ni_{0.56}S$. The components were accurately weighed and placed in a vycor tube which was evacuated and sealed before being slowly heated to 500°C. This temperature was maintained for 48 h. The tubes were removed from the furnace and quenched rapidly in iced water. The mss was ground and placed in a fresh tube, and reheated to 500°C for a further 48 h. The sample was again quenched and heated at 500°C for a further 15 days. After quenching and grinding, sufficient sulfur was added to the mss of $Fe_{0.28}Ni_{0.56}S$ to achieve the $FeNi_2S_4$ composition. The vapor space in the tube was taken up with a silica rod. The evacuated and sealed tube was heated for 12 weeks at 300°C. After quenching, the sample was passed through Brass Endecott Laboratory Test Sieves to isolate the 45–75 μm fraction.

2.2. Techniques

Iron, nickel and sulfur were determined by wet chemical analysis.

Simultaneous TG–DTA experiments were performed using a Stanton Redcroft 780 Thermal Analyser interfaced with an IBM-compatible personal computer. Approximately 7 mg of sample was weighed into an alumina crucible (3.8 mm internal diameter,

3.0 mm height), placed in the TG–DTA apparatus and heated at 10°C min^{-1} in dried air flowing at 40 mL min^{-1}.

TG–DSC–FT–IR experiments were performed using a Netzsch STA-409 TG–DTA instrument interfaced with a Bruker IFS 55 FT–IR spectrometer fitted with an MCT (Hg–Cd–Te) detector. Approximately 5 mg of sample was placed into an alumina crucible. The instrument was evacuated and purged with dry air, and the sample heated at 10°C min^{-1}. The evolved gases were fed into the FT–IR spectrometer through a heated transfer line at 200°C and a heated light pipe fitted with outer (KBr) and inner (ZnSe) windows; 20 scans were averaged every 5 s.

XRD experiments were performed using a Siemens D500 Bragg–Brentano diffractometer fitted with a copper X-ray tube, rotating specimen stage and sodium iodide detector.

FT–IR spectra of solid samples were recorded with a Perkin-Elmer 1720 FT–IR spectrometer fitted with a TGS detector and a potassium bromide beam splitter. Forty repetitive scans were taken of each sample at a mirror velocity of 0.2 cm s^{-1} and resolution of 4 cm^{-1} throughout the range 4000–400 cm^{-1}. Samples were prepared using a Wig-L-Bug grinder/mixer manufactured by Crescent Dental Mfg. Co, Illinois, USA. It was fitted with an agate vial and ball pestle. Approximately 4 mg of sample was mixed with 500 mg of spectroscopic grade potassium bromide (Uvasol, Merck Chemical Co.) for 10 min in the Wig-L-Bug. Approximately 200 mg of the mixture was pressed into a disk. Data were processed using OPUS/IR Version 1.4.17 spectroscopic software by Bruker Analytische Messtechnik GmBH.

Microscopy was performed on samples embedded in epoxy resin. Optical micrographs of the polished samples were obtained using a Nikon Labophot 2 optical microscope fitted with an NCB 11 filter and a Nikon FX-35W 35 mm camera. The samples were carbon coated for analysis using SEM. SEM was performed on a JEOL JSM-6400 scanning electron microscope fitted with a LINK X-ray Energy Dispersive Spectrometer (EDS) detector. EDS data were processed using SPEED spectral analysis software [7] and RECAL2 [8].

3. Results and discussion

3.1. Sample characterization

The results of wet chemical analysis of the synthetic violarite indicated that the stoichiometry of the sample, $Fe_{1.01}Ni_{2.17}S_4$, was close to that of ideal violarite. Backscattered electron (BSE) micrographs (Fig. 2(a)) obtained by SEM revealed angular particles with the majority of particles containing a single phase. A slightly darker phase was evident in some particles, which was judged by its relative surface to be at about the 5% level. EDS analysis indicated an even distribution of Fe and Ni throughout the lattice structure and confirmed the presence of two phases. The most common phase had an average formula of $Fe_{1.13}Ni_{2.01}S_4$. The other phase appeared to be mss with an average formula of $Fe_{0.34}Ni_{0.62}S$. XRD examination of the sample indicated that violarite was the major phase present, with a calculated cubic unit cell

parameter of $a = b = c = 9.46$ Å. This value corresponded well with a unit cell dimension of 9.463Å for $FeNi_2S_4$ [9]

3.2. Oxidation experiments

A typical TG–DTA trace for the oxidation of synthetic violarite is presented in Fig. 1. A mass loss in the temperature range 405–475°C was accompanied by an exotherm in the temperature range 380–510°C. A mass gain appeared between 475 and 585°C associated with an exothermic peak between 510 and 650°C. A series of consecutive mass losses appeared in the temperature range 585–840°C, and can be separated into four stages: 585–670, 670–725, 725–785 and 785–840°C. Two substantial exotherms featured in the temperature ranges 650–715 and 800–860°C. A broad endotherm commenced at 755°C, and was overlaid by a small, sharp endotherm which appeared at 790°C.

Partially oxidized product was collected at the temperatures indicated in Fig. 1. Activity in the DTA curve and changes in the slope on the TG curve were used to select these points. When the selected temperature was attained, the heating program was suspended and the atmosphere immediately changed to nitrogen. The sample and furnace were allowed to cool to ambient temperature.

The partially oxidized samples were analyzed by various techniques including XRD, FT–IR, SEM and EDS. BSE micrographs of partially oxidized samples are shown in

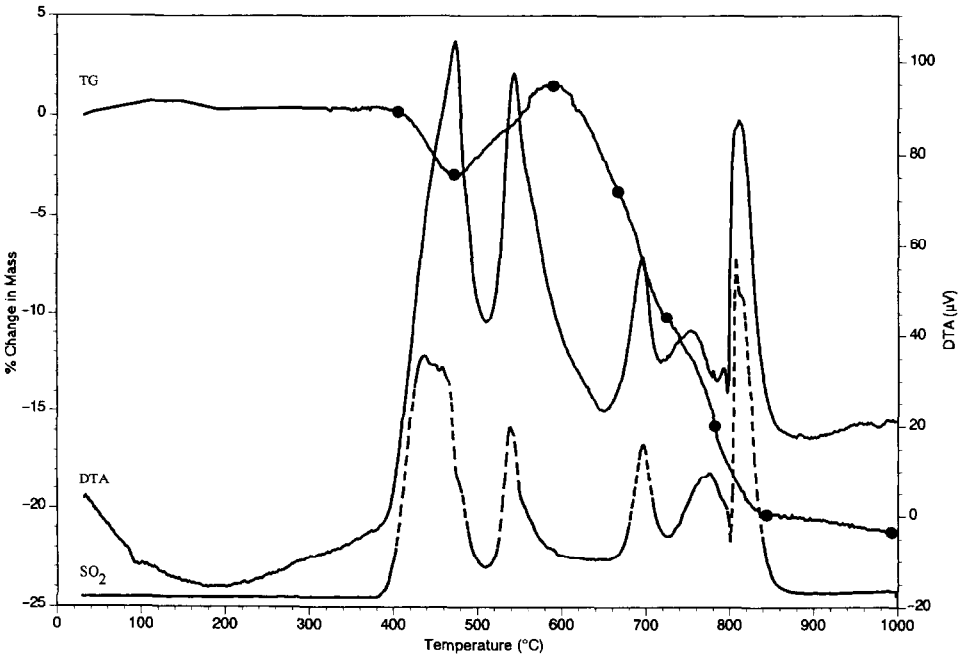

Fig. 1. TG–DTA–SO_2 curve for the oxidation of violarite. Collection points (●) are indicated on the TG curve. 7mg sample, 10°C min^{-1} heating rate, air atmosphere, particle size 45–75 μm.

Fig.2(a)–(i). FT–IR spectra of partially oxidized samples are presented in Fig. 3, and the phases identified by XRD and FT–IR in Fig. 4.

3.3. Reaction sequence

Endothermic drift was evident below 380°C (Fig. 1), but was not associated with any mass change. BSE micrographs at 405°C (Fig. 2(b)) showed that the majority of particles remained unreacted. However, some particles did show signs of reaction in the form of a dark porous product at the solid/gas interface. XRD analysis indicated that violarite was the major phase present, with mss as a possible minor phase. FT–IR analysis of this sample (Fig. 3, 405°C) showed peaks at 996 and 984 cm^{-1} which were indicative of iron(II) sulfate and nickel sulfate respectively [10]. Hence up to 405°C, minor sulfation of the external surface of the particle occurred.

The first stage of oxidation occurred in the temperature range 405–475°C, with a mass loss of 3.24%. This was accompanied by an exothermic peak and the evolution of SO_2. The BSE micrographs of samples taken at 475°C (Fig. 2(c)) showed the continued formation of the dark porous phase on the exterior of the particles. Because of the porosity, it was difficult to focus the electron beam on only solid material, and analytical values gave low weight percent totals. However it clearly indicated that this phase was iron-rich. A dense grey phase was evident at the interface between the porous rim and the sulfide core in some particles. Analysis revealed that it was iron-rich in

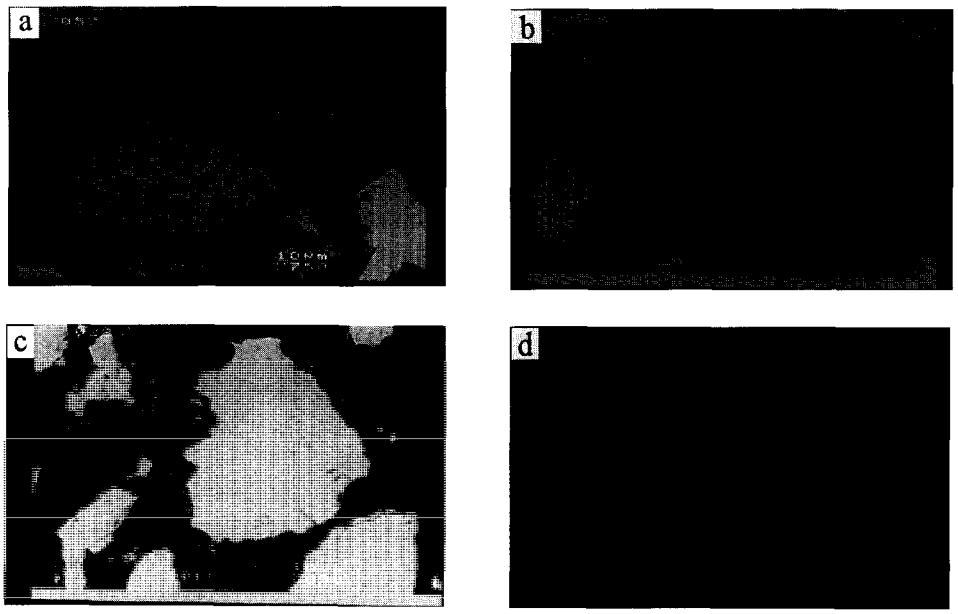

Fig. 2. Backscattered electron micrographs of partially oxidized samples of violarite. Collection temperatures are: (a) unreacted, (b) 405, (c) 475, (d) 585, (e) 670, (f) 725, (g) 785, (h) 840, (i) 1000 °C.

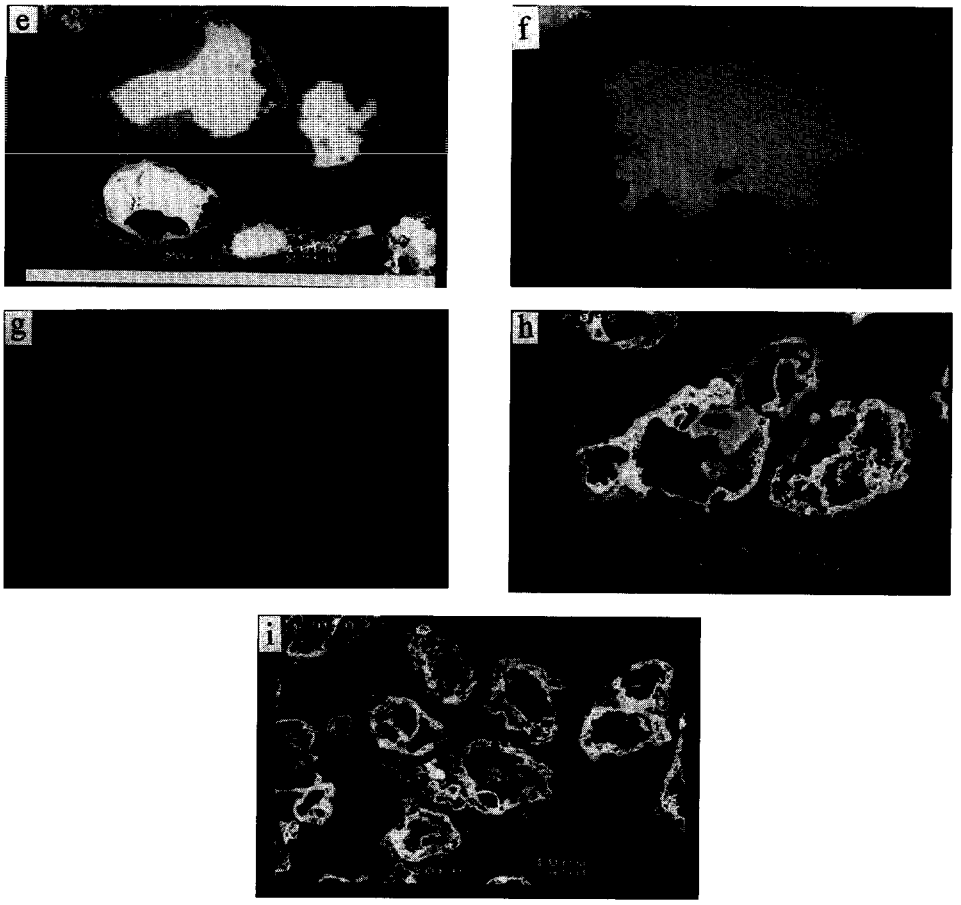

Fig. 2 (*Continued*)

comparison to the sulfide core. EDS analysis indicated that the sulfide core contained variable iron and nickel values, which ranged from $Fe_{0.16}Ni_{0.84}S$ to $Fe_{0.35}Ni_{0.61}S$, with an average composition of $Fe_{0.28}Ni_{0.71}S_{1.00}$. There was a general trend of decreasing iron concentration from the center of the mss to the outer edge of the mss boundary, the nickel:iron ratio in the center of the particle was 2:1 whilst near the sulfide–oxide boundary it was 5:1. The proportion of iron increased markedly as the sulfide boundary was crossed. These results indicated that significant ion migration of iron had occurred during the oxidation process.

XRD analysis of the product at 475°C revealed a strong match with the mss pattern and a minor match with violarite. There was still no evidence of sulfates in the XRD pattern, although $FeSO_4$ and $NiSO_4$ were detected using FT–IR (Fig. 3, 475°C). It was likely that the sulfate species were amorphous and difficult to detect using XRD [11, 12]. Iron (III) sulfate was also detected in the spectrum and identified using the

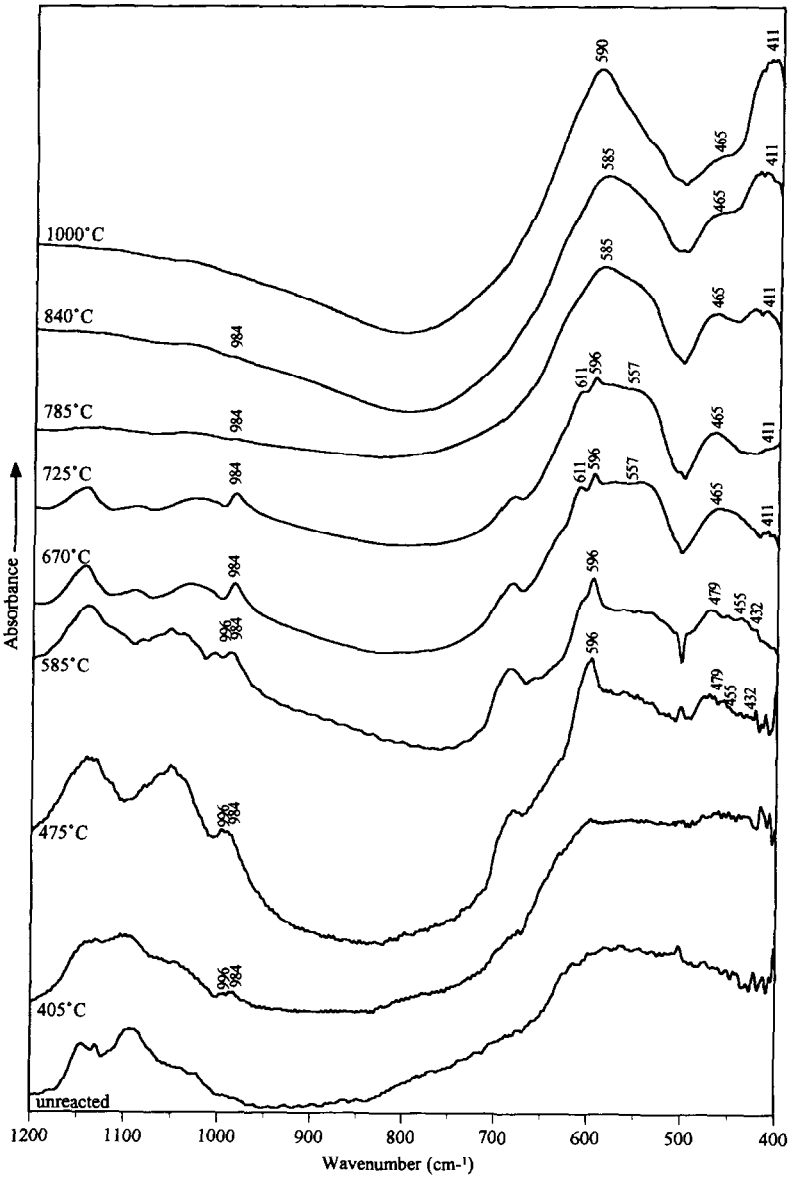

Fig. 3. FT-IR spectra of partially oxidized violarite at various temperatures.

peaks at 455 and 433 cm^{-1} [12] as well as by comparison with a reference sample.

According to the predominance diagram by Craig [3], a sample with the stoichiometry used in this study should reach its stability limit in a sealed tube at approximately 380°C. This is in the same temperature region as the commencement of the mass loss at 405°C observed in the TG trace. In a sealed tube, violarite is reported to

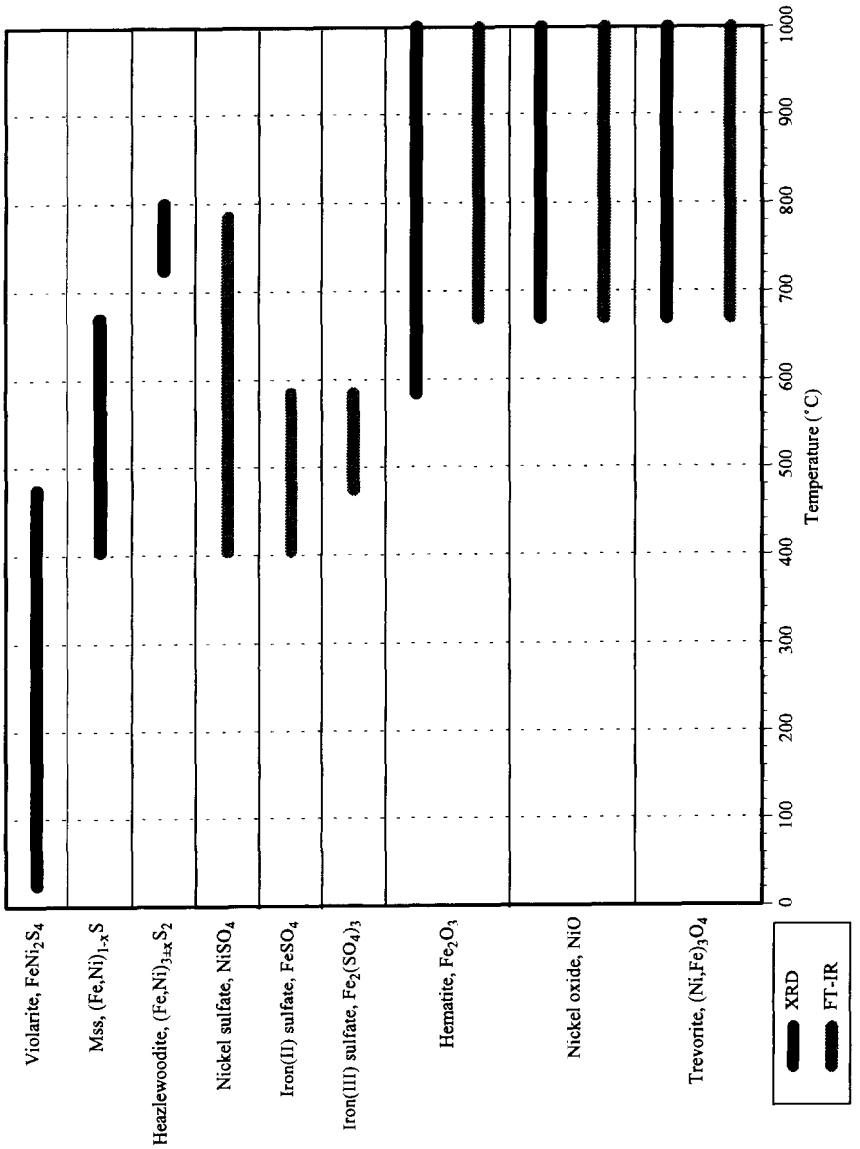

Fig. 4. Phases identified by XRD and FT-IR in partially oxidized violarite as a function of temperature.

decompose to pyrite (Fe, Ni) S_2, vaesite (Ni, Fe) S_2 and mss $(Fe, Ni)_{1-x}S$ with iron and nickel in the ratio of 1:2.4 [3]. In this study, the ratio of metal atoms in the mss at 475°C averaged 1:2.5. The ternary phase diagrams at 450 and 500°C [3] confirmed that the observed stoichiometries lie within the mss zone. Pyrite and vaesite were not detected by XRD, but this is probably because the samples were in an open environment so that any evolved sulfur was swept away and converted to sulfur dioxide. Thus there was no opportunity for the evolved sulfur to recombine to produce vaesite and pyrite.

On the evidence collected, the mass loss and exotherm found in the temperature range 405–475°C were the result of the reactions

$$(Fe, Ni)_3S_4 \rightarrow (Fe, Ni)_{1-x}S + S \rightarrow SO_2$$

violarite mss

Sulphation reactions continued, with the formation of iron (III) sulfate in addition to more iron (III) and nickel (II) sulfates.

In the temperature range of 475–585 °C, a mass gain of 4.53% was observed accompanied by an exothermic reaction and the evolution of SO_2. The BSE micrographs (Fig. 2(d)) and optical microscopy of samples taken at 585°C showed multiple phases in the rims surrounding the sulfide core, although mss was still the major phase. Analysis of the unreacted core by EDS revealed a nickel-rich mss phase with a constant metal:sulfur ratio of 1.02 and nickel:iron ratios that ranged from 5.9:1 to 3.2:1. The dense grey phase adjacent to the sulfide core had increased in thickness and almost encircled the sulfide core. EDS analysis indicated it was an iron-rich phase with significant amounts of nickel and sulfur, probably indicating the presence of nickel and iron sulfates. This grey phase was encased in a black porous rim that was scattered with red and orange colored phases. Under polarized light, the black porous phase had brilliant red internal reflections typical of hematite. The porous rim surrounding the particles was found by EDS to be an iron-rich phase. All of these strongly suggested that the porous phase was hematite.

XRD indicated a strong match with the intermediate synthesis product, mss, together with hematite, although no nickel oxide was detected. The FT–IR spectrum (Fig. 3, 585°C) showed the identifying peaks of nickel (II) sulfate, iron (III) sulfate and iron (II) sulfate.

The evolution of sulfur dioxide can be assigned to the oxidation of sulfide and was responsible for the exothermic effect found in this range. Some of the evolved sulfur dioxide would react with metal oxides to produce sulfates and cause the mass gain. However, it is not easy to assign the reaction to the oxidation of mss as this reaction would produce both nickel oxide and hematite, and the former was not detected by any of the characterization methods used. One possibility is that the diffusion of iron towards the rim produced very iron-rich sulfides which oxidized as air diffused into the particle, with the formation of hematite and a minor quantity of nickel oxide which was not detected by XRD. Pyrrhotite, $Fe_{1-x}S$, for example, is reported to oxidize in this temperature range with the formation of hematite [13]. Alternatively, a minor amount of nickel oxide may have been completely sulfated by the relatively

large quantity of sulfur dioxide released by the oxidation reaction. It is therefore difficult to write equations to describe the reactions taking place in this temperature range.

A mass loss of 5.52% was observed between 585 and 670°C. The baseline of the DTA drifted endothermically. A peak was not evident in the evolved gas spectrum, although the curve did not return to its horizontal baseline. This implied that a slow but steady evolution of SO_2 had occurred over the temperature interval. Examination by BSE of samples taken at 670°C (Fig. 2(e)) showed that the particles still contained 60–70% unreacted sulfide. EDS analysis of the sulfide core gave an average mss composition of $Fe_{0.05}Ni_{1.08}S$ so that the nickel: iron ratio was now 20:1. This had decreased significantly from the ratios at 585°C and confirmed that iron had migrated to the reaction front. A new dense grey phase was apparent adjacent to the sulfide core; this was iron-rich and extremely sulfur deficient. When oxygen was included in the mass percent totals, the mass empirical formula implied the phase was trevorite, $(Fe,Ni)_3O_4$. This was likely to be the product of direct oxidation of the mss phase, with the replacement of sulfur by oxygen. The BSE micrographs also showed that the porous oxide rim was expanding and was iron-rich with little sulfur detected. As before, strong red reflections indicative of hematite were observed by optical microscopy under polarizing conditions. The adjacent phase was probed, producing evidence of nickel, iron and sulfur in various metal ratios. The iron was likely to be associated with hematite while the nickel may exist as nickel sulfate, nickel oxide or be associated with trevorite. Holes appeared at the intersection of the sulfide core and the oxide rim, indicating shrinkage of the sulfide core.

At 670°C the XRD pattern confirmed the presence of hematite, trevorite, and nickel oxide but mss continued to dominate the pattern. The FT–IR spectrum (Fig. 3, 670°C) identified hematite, nickel oxide, trevorite and nickel sulfate in the sample. The mass gain expected from the formation of nickel sulfate was not observed due to the mass loss associated with the decomposition of iron sulfates, which was the dominant reaction in the temperature range 585–670°C.

In the temperature range 670–725°C, there was a 6.17% mass loss and an exothermic peak coinciding with the evolution of SO_2. The BSE micrographs of samples taken at 725°C (Fig. 2(f)) clearly showed the outer oxide rim and an inner rim that was adjacent to the core. The holes in this interface had increased in both size and number. Analysis of the sulfide core by EDS revealed a nickel-rich sulfide that approximated to high heazlewoodite, $Ni_{3\pm x}S_2$, where $0.2 < x < 0.7$. Less than 2.5% iron was detected. The sulfide core appeared to be shrinking as the oxidation progressed leaving large holes at the sulfide/oxide interface. The light grey inner rim gave an iron-rich/sulfur-deficient total. The darker phase in the rim gave values that were only slightly iron-rich and may indicate trevorite. The sulfur dioxide may be partially consumed in sulfating nickel oxide. The XRD pattern indicated that heazlewoodite, hematite, trevorite and nickel oxide were present. The FT–IR spectrum (Fig. 3, 725°C) revealed nickel sulfate, trevorite, nickel oxide and hematite.

The ternary phase diagram at 650°C [3] showed a tie line from the mss region to the heazlewoodite region associated with the loss of sulfur. Hence the mass loss in this temperature range can be attributed to the loss of sulfur as the decomposition

temperature of mss is exceeded, with the production of heazlewoodite. The oxidation of the evolved sulfur will give rise to the associated exotherm. In addition, some of the heazlewoodite may be oxidized to nickel oxide, which was detected for the first time by XRD. The formation of heazlewoodite was the chief reaction in this temperature range

$$(Fe,Ni)_{1-x}S \rightarrow (Ni,Fe)_{3\pm x}S_2 + S \rightarrow SO_2$$

mss heazlewoodite

The temperature range of 725–785°C had a mass loss of 6.07% and was associated with an endotherm between 750 and 785°C and the evolution of sulfur dioxide. BSE micrographs of samples taken at 785°C (Fig. 2(g)) showed that the holes formed between the rim and the core had increased in number and size. In some cases the core appeared suspended within an oxide shell. A few particles consisted of only a shell. However, the majority of particles retained some sulfide core that was previously identified as high heazlewoodite. The BSE image still showed a multiphase rim that was too porous for EDS analysis. Heazlewoodite, nickel oxide, hematite and trevorite were all identified by XRD. Nickel sulfate was still evident in the FT–IR spectrum at 785°C (Fig. 3, 785°C), although the spectrum was becoming dominated by hematite and trevorite. In a separate TG–DTA experiment, nickel sulfate was heated at 10°C min^{-1} in air, and found to commence decomposition at 725°C which was complete by 840°C. The evolution of sulfur dioxide resulted from this decomposition, as well as the formation of more nickel oxide. Hence the mass loss and endotherm appear to be related to be decomposition of nickel sulfate.

The final mass loss of 3.82% occurred between 785 and 840°C accompanied by an exotherm and evolution of a significant amount of sulfur dioxide. The BSE micrographs of samples taken at 840°C (Fig. 3(h)) showed that no sulfide core remained. The decomposition of nickel sulfate was concluded in this range. A small endotherm, which could be attributed to the melting point of heazlewoodite, was located at 785°C prior to the onset of the exotherm. Stoichiometric heazlewoodite is reported to melt incongruently in the temperature range 783–785°C [14]. The experimentally determined melting temperature further supports the high purity of the heazlewoodite, since increasing concentrations of iron substitution move the melting temperature to higher values [2]. The rapid oxidation of these phases produced an exotherm, a mass loss, and the evolution of SO_2. The XRD pattern indicated that nickel oxide, hematite and trevorite were present. Trevorite dominated the FT–IR spectrum (Fig. 3, 840°C), and obscured any peaks due to hematite or nickel oxide. A small peak associated with nickel sulfate was observed at 840°C.

At 1000°C, the sample contained hematite, nickel oxide and trevorite (see Figs. 2(i), 3(1000°C) and 4).

4. Conclusions

The reaction scheme for the oxidation of violarite has been established. Although the oxidation process involved the formation of the usual oxidation products of sulfides,

such as sulfates and oxides, there were some novel features.

Some of the reaction sequence was controlled by the non-oxidative thermal decomposition of the sulfide to form a new sulfide compound. This occurred twice, the first time with the decomposition of violarite to mss at 405°C; and then at 670°C with the decomposition of mss to form heazlewoodite. In both cases sulfur was evolved with subsequent oxidation, giving rise to associated exothermic events.

The next feature was the preferential migration of iron from the sulfide core to the particle rim, where it underwent sulfation and oxidation. The nickel:iron ratios in the sulfide core changed from 2:1 at 405°C to 20:1 at 670°C, whereas in the oxide rim only iron was detected. The phenomenon of iron migration had previously been qualitatively reported during the roasting of pentlandite [15,16]. Beyond the decomposition of violarite to mss, the system behaved essentially as two discrete phases, with preferential oxidation of iron sulfide components in the lower temperature ranges, followed by the oxidation of the remaining nickel sulfide phases.

The formation of oxide and sulfate coatings gave significant protection against oxidation to the sulfide core, and mss and then heazlewoodite were the predominant phases present in the particles up to the temperature at which the heazlewoodite melted. Rapid oxidation of the liquid phase and the disappearance of sulfide followed.

References

[1] E.H. Nickel, AusIMM Conf., May 1973.
[2] G. Kullerud, Carnegie Inst. Wash. Year Book, 62 (1963) 175.
[3] J.R. Craig, Amr. Mineral., 56 (1971) 1303.
[4] R.A. Keele and E.H. Nickel, Econ. Geol., 69 (1974) 1102.
[5] E.H. Nickel, J.R. Ross and M.R. Thornber, Econ. Geol., 69 (1974) 93.
[6] J.G. Dunn and L.C. Mackey, J. Therm. Anal., 37 (1991) 2143.
[7] N.G. Ware, Computers and Geosciences, 7 (1981) 167.
[8] B.J. Griffin, J.R. Muhling, G.W. Carrol and N.M.S. Roch, Amr. Mineral., 76 (1991) 295.
[9] D.J. Vaughn and J.R. Craig, Mineral Chemistry of the Metal Sulfides, Cambridge University Press, Cambridge, 1978, p. 357.
[10] S.D. Ross, in V.C. Farmer (Ed), The Infrared Spectra of Minerals, Monograph 4, Mineralogical Society, London, 1974, p. 428.
[11] J.G. Dunn, W. Gong and D. Shi, Thermochim. Acta, 208 (1992) 293.
[12] J.G. Dunn, G.C. De and B.H. O'Connor, Thermochim. Acta, 145 (1989) 115.
[13] T. Kennedy and B.T. Sturman, J. Therm. Anal., 8 (1975) 329.
[14] G. Kullerud and R.A. Yund, J. Petrol., 3 (1962) 126.
[15] P.G. Thornhill and L.M. Pidgeon, J. Metals, 9 (1957) 989.
[16] J.G. Dunn and C.E. Kelly, J. Therm. Anal., 18 (1980) 147.